Cancer tolerance to chromosomal instability is driven by Stat1 inactivation *in vivo*

Michael Schubert[1,2,3,*,#], Christy Hong[1,*], Laura J. Jilderda[1,*], Marta Requesens Rueda[1,4,*], Andréa E. Tijhuis[1,|], Judith E. Simon[1,|], Petra L. Bakker[1], Jon L. Cooper[5,6,7], Aristi Damaskou[5,6], René Wardenaar[1], Bjorn Bakker[1], Sahil Gupta[1], Anouk van den Brink[1], Lorena Andrade Ruiz[1], Miriam H. Koster[8], Sameh A. Youssef[9], Danielle Luinenburg[1], Alex Strong[7], Thomas Engleitner[10], Hannes Ponstingl[7], Gerald de Haan[1], Alain de Bruin[8,9], Roland Rad[10], Hans W. Nijman[4], René H. Medema[2], Marcel A.T.M. van Vugt[11], Marco de Bruyn[4], Diana C.J. Spierings[1], Maria Colomé-Tatché[3], George S. Vassiliou[5,6,7], Floris Foijer[1,#]

[1]European Research Institute for the Biology of Ageing, University of Groningen, University Medical Center Groningen, 9713 AV, Groningen, the Netherlands

[2]Division of Cell Biology and Cancer Genomics Center, Netherlands Cancer Institute, Plesmanlaan 121, 1066 CX, Amsterdam, the Netherlands

[3]Institute of Computational Biology, Helmholtz Zentrum München, German Research Center for Environmental Health, Neuherberg, Germany

[4]Department of Obstetrics and Gynaecology, University of Groningen, University Medical Center Groningen, 9713 AV, Groningen, the Netherlands

[5]Wellcome–Medical Research Council (MRC) Cambridge Stem Cell Institute, Cambridge, United Kingdom;

[6]Department of Haematology, Cambridge University Hospitals National Health Service (NHS) Trust, Cambridge, United Kingdom

[7]Wellcome Sanger Institute, Wellcome Genome Campus, Hinxton, Cambridge, United Kingdom

[8]Department of Pediatrics, University of Groningen, University Medical Center Groningen, 9713 AV, Groningen, the Netherlands

[9]Dutch Molecular Pathology Center, Department of Biomolecular Health Sciences, Utrecht University, Faculty of Veterinary Medicine, 3584 CL, Utrecht, the Netherlands.

[10]Institute of Molecular Oncology and Functional Genomics, School of Medicine, Technische Universität München, 81675, Munich, Germany

[11]Department of Medical Oncology, University of Groningen, University Medical Center Groningen, 9713 AV, Groningen, the Netherlands

[*] These authors contributed equally

[#] To whom correspondence should be addressed: m.schubert@rug.nl, f.foijer@umcg.nl

NOTE: High Resolution Figures at the end of the manuscript

Abstract

Chromosomal instability is a hallmark of cancer, but also an instigator of aneuploidy-induced stress, reducing cellular fitness. To better understand how cells with CIN adjust to aneuploidy and adopt a malignant fate *in vivo*, we performed a genome-wide mutagenesis screen in mice. We find that specifically aneuploid tumors inactivate Stat1 signaling in combination with increased Myc activity. By contrast, loss of p53 is common, but not enriched in CIN tumors. Validation in another tissue type confirmed that CIN promotes immune cell infiltration, which is alleviated by Stat1 loss combined with Myc activation, but not with p53 inactivation, or Myc activation alone. Importantly, we find that this mechanism is preserved in human aneuploid cancers. We conclude that aneuploid cancers inactivate Stat1 signaling to circumvent immune surveillance.

Introduction

Chromosomal instability (CIN) is a phenomenon characterized by frequent chromosome missegregation events, resulting in cells displaying structural and/or chromosomal abnormalities, *i.e.* aneuploidy (*1*). CIN is a hallmark of cancer and associated with tumor recurrence, metastasis and drug resistance and thus poor patient prognosis (*2–5*). However, in untransformed cells, CIN and aneuploidy impair cellular fitness, evidenced by reduced proliferation, decreased transformation potential, a deregulated cellular metabolism, and senescence (*6–8*). This apparent contradiction is also known as the aneuploidy paradox (*9*) and implies that aneuploid cancer cells need to overcome certain barriers to cope with aneuploidy. As aneuploid cancer cells might rely on such coping mechanisms for their survival, targeting these mechanisms could provide a powerful strategy for treating these cancers. However, to develop such therapies, we need to better understand the barriers that aneuploid cells need to overcome to become malignant.

Over the past decade, several aneuploidy-induced stresses have been identified, including proteotoxic stress (*4*, *7*, *10*), metabolic stress (*8*, *11*), and an inflammatory response (*11–15*). Reducing these stresses has been found to improve the overall cellular fitness of aneuploid cells while exacerbating these stresses reduces their fitness. For instance, neuronal cells from individuals with Down syndrome exhibit increased expression of the ubiquitin-mediated proteasome system, and are extremely sensitive to factors that exacerbate proteotoxic stress such as compounds that trigger ER stress (*16*). Similarly, aneuploid yeast cells are extremely sensitive to inhibition protein ubiquitination, as this exacerbates aneuploidy-induced proteotoxic stress (*17*). While such studies have greatly improved our understanding of how individual cells cope with aneuploidy, most were performed in cultured mammalian cells or yeast and therefore cannot fully capture the complete process of tumorigenesis.

To better understand how CIN and aneuploidy lead to cancer, mouse models were generated with mutations that lead to decreased mitotic fidelity (*18*, *19*), which revealed that in most genetic backgrounds CIN is a poor instigator of cancer. However, inactivation of p53, a common event in cancer, promotes propagation and transformation of tetraploid cells and the formation of aneuploid tumors (*20*). Indeed, loss of p53 and CIN have been shown to collaborate in tumorigenesis in various models (*12*, *21*, *22*). However, the exact role of p53 in preventing the outgrowth of aneuploid cells is not fully understood, as for instance expression of a functional p53 does not impair propagation of all aneuploid cells *per se* (*23*, *24*).

Complementarily, observational studies of large human cancer cohorts have identified an increased mutational load and decreased leukocyte infiltration in more aneuploid tumors (*25*). Somatic copy number aberrations have been linked to aneuploidy-specific immune evasion, *e.g.* by gaining certain oncogenes or loss of heterozygosity at the HLA locus (*26*). Gene expression signatures have been developed to estimate CIN in human tumors (*27*), but there is some disagreement about the extent they, instead, reflect other processes like CIN-independent proliferation (*28*, *29*). Finally, multi-region sequencing efforts have employed tumor heterogeneity to conclusively link oncogene and antigen shuffling to chromosomal instability (*30*, *31*). In particular, metastatic samples showed a CIN-driven recurrent amplification of 8q24, encompassing *MYC*, or 11q13, encompassing *CCND1* (*31*).

Both the functional as well as the observational studies have provided valuable insights into how cancer cells cope with stresses introduced by aneuploidy or chromosomal instability. However, to our knowledge there has not been an unbiased and comprehensive comparison of how different cancer drivers enable euploid or aneuploid/CIN transformation into aggressive tumors *in vivo*. Here we present a genome-wide transposon mutagenesis screen in the hematopoietic system of isogenic mice with or without induced CIN. We find that p53 mutations enable both euploid and aneuploid cancer growth, while a combination

of Stat1 inactivation and Myc amplification is a driver unique to the CIN phenotype. We further provide strong evidence that this mechanism extends to other cancer types in mice, and is consistent with observations in The Cancer Genome Atlas (TCGA) cohorts.

Results

An *in vivo* insertional mutagenesis screen using a genetically engineered CIN mouse model

Chromosomal instability discriminates cancer cells from healthy cells. Therefore, selectively targeting CIN could provide a powerful strategy to treat many cancers. To develop such therapies, we need to understand which features are unique to CIN cancers. We performed an *in vivo* genetic screen to compare the cancer-driving genes between tumors with and without a CIN phenotype in an otherwise isogenic setting. We took advantage of the fact that CIN alone is a poor instigator, yet a powerful accelerator of cancer when combined with cancer-predisposing mutations (*12*, *21*, *22*, *32*, *33*). To limit CIN and mutagenesis to a single tissue, we combined a conditional driver of CIN with a conditional transposon mutagenesis system. For this, we crossed mice harboring our well-characterized conditional Mad2$^{f/f}$ allele (*11*, *22*) with mice that carry a cassette of 15 PiggyBac (PB) transposons on chromosome 16 and a Lox-Stop-Lox PB-Transposase, allowing for tissue-specific activation of transposon mutagenesis (*34*, *35*). The PB transposable elements in this model can activate or inactivate genes depending on the integration site (**Fig. 1a**) (*34*, *35*). We chose to target the hematopoietic system as 1) approximately half of human hematopoietic cancers aneuploid (*36*), allowing us to compare the drivers between CIN and non-CIN tumors and 2) hematopoietic tumors in mice display a relatively short latency. We therefore crossed our mice into an Mx1-Cre background in which Cre-recombinase can be activated in the hematopoietic compartment through PolyI:PolyC (pI:pC) injections (**Fig. 1a**). Two cohorts of mice were treated: 1) 45 Transposon; Mx1-Cre mice and 2) 104 Mad2$^{f/f}$;Transposon;Mx1-Cre mice. Both cohorts were monitored for tumorigenesis alongside two control groups (pI:pC-treated Mad2$^{f/f}$;Mx1-Cre mice and untreated Mad2$^{f/f}$;Transposon;Mx1-Cre mice). Treated Mad2$^{f/f}$;Transposon;Mx1-Cre mice showed a median survival of 13 months compared to 18 months for Transposon;Mx1-Cre mice, confirming that CIN is a powerful accelerator of tumorigenesis, also in this background (**Fig. 1b**). Untreated Mad2$^{f/f}$;Transposon;Mx1-Cre mice developed sporadic hematopoietic malignancies as well, but with longer latencies, consistent with sporadic leaky Mx1-Cre expression. Histology and flow cytometry analysis of the malignancies revealed that about half were poorly differentiated B-cell tumors, and the other half were either of myeloid or T-cell origin (**Fig. S1a-d**, **Fig. 1b**). We quantified Mad2 loss in Mad2$^{f/f}$ tumors by quantitative genomic PCR, RT-PCR and Western blot assays, and confirmed that most Mad2$^{f/f}$ tumors had indeed lost Mad2 expression (**Fig. S1e-i**).

To quantify aneuploidy, we performed shallow whole genome sequencing for all tumors, which showed that all Mad2$^{f/f}$ tumors, except one, and only a few Transposon-only tumors were aneuploid (**Fig. 1c**). As expected, tumors with only heterozygous inactivation of Mad2 were not affected by the CIN phenotype. In terms of whole-chromosome copy number changes, we find that chromosome 15 (harboring *Myc*) was the most frequently amplified in the CIN-high tumors, and the only chromosome with recurrent amplifications of more than one additional copy. The next most frequently amplified was chromosome 6, harboring *Kras*. Both *Myc* and *Kras* are potent oncogenic drivers, supporting the hypothesis that CIN enables tumors to shuffle their genome content to select clones with a favorable oncogene to tumor-suppressor gene ratio (*26*, *37*). We also observe recurrent amplifications of the region of chromosome 16 that harbors *Erg*, a well-known driver of leukemias (*38*). Stratification per tumor type revealed that myeloid malignancies were rarely aneuploid, and that T-ALLs on average were more aneuploid than B-cell precursor malignancies. We did not observe a sex bias for switching efficiency or the resulting aneuploidy level.

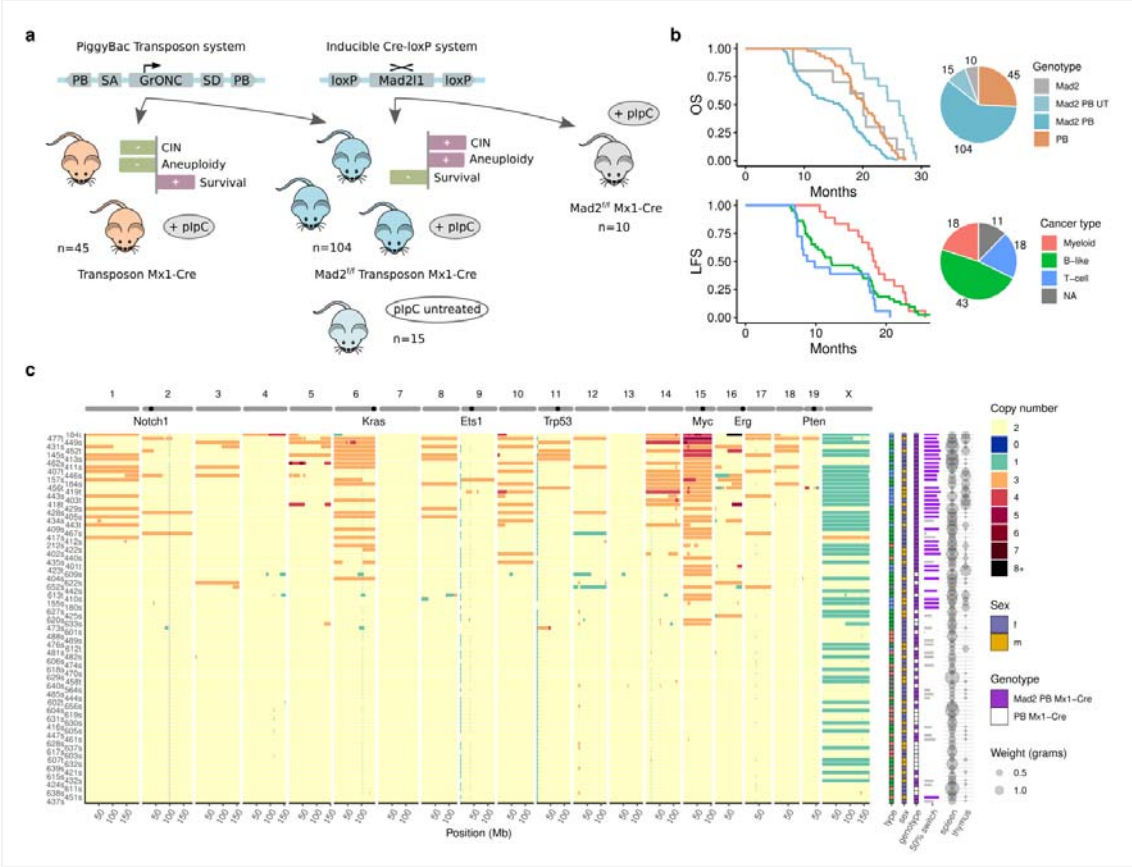

Fig. 1. Experimental setup and cohort overview. **(a)** Treatment scheme of mice with either PiggyBac insertional mutagenesis alone or in combination with homozygous Mad2$^{f/f}$ allele. Both genetic modifications are activated via pI:pC. Controls include untreated (UT) mice and Mad2$^{f/f}$ alone. **(b)** Overall survival by genotype (OS, top) or Leukemia free survival (LFS) by consensus tumor type from histology and FACS (bottom). Combined Mad2$^{f/f}$ PB constitutes the largest part of the cohort, followed by PB-only. The combined genotype is the most aggressive and untreated mice show the longest survival. Both individual genotypes fall in between. For tumor types, T-ALLs are the most aggressive, followed by B-like tumors and myeloid tumor bearing mice survive the longest. Tumor types are enriched in the respective genotypes. **(c)** Average DNA copy number patterns across the whole cohort, including tumor type, sex, genotype, switching efficiency, and tumor weight in both spleen and thymus. Chromosome 15 is the most amplified, followed by chromosome 6. T-ALLs are the most aneuploid, myeloid the least. B-like tumors span the whole range. Aneuploidy is strongly correlated with the Mad2$^{f/f}$ genotype, most tumors of which are also homozygously switched. Unswitched tumors are markedly more euploid, with a single exception of a switched tumor. Heterozygous switching does not confer CIN (grey bars).

Transposon insertions and RNA-seq reveal a CIN-dependent Stat1/Myc axis

We sequenced the transposon integration sites and mapped Common Insertion Sites (CIS), *i.e.* transposon integrations that affected a gene or region more often than would be expected by chance, across the entire mouse cohort (**Fig. 2a**). Among the most affected genes were *Trp53*, *Crebbp*, and the known hematopoietic drivers *Ets1*, *Erg*, *Ikzf1*, *Foxn3*, *Pten*, and *Runx1* (**Fig. S2a**), consistent with a previous hematopoietic screen (*35*). We also quantified whether a CIS is CIN-specific by testing for a difference in aneuploidy in inserted *vs.* non-inserted samples as aneuploidy correlates well with karyotype heterogeneity in single-cell DNA sequencing, an established measure for CIN (**Fig. 2b**). Among the most significantly enriched genes were *Erg*, *Hs6st3*, *Dnm3*, and *Stat1* (**Fig. S2b**). We further used a subnetwork identification algorithm on protein interactions to narrow down our list of hits to the most important altered biological processes. We retained most of our top hits, suggesting they may target a common process (**Fig. S2c-d**). Ranking the cleaned-up list by degree of aneuploidy, we found *Erg* and *Stat1* as the most CIN-specific

hits, *Ets1* and *Trp53* as non-specific, and *Pias1* as the most euploid-specific hit (**Fig. 2c**). Interestingly, Pias1 is a known inhibitor of Stat1 (*39*), also by name (Protein inhibitor of activated Stat1). This, together with the fact that Stat1 is central to both the cohort and the CIN-specific subnetwork (**Fig. 2d**, **Fig. S2c-d**), leads us to conclude that inactivation of Stat1 is likely the main requirement for hematopoietic tumors to tolerate CIN. Interestingly, insertions involving Stat1 interactors were generally enriched in euploid tumors, the opposite of Stat1 itself (**Fig. S2d**), suggesting that they may also act as inhibitors.

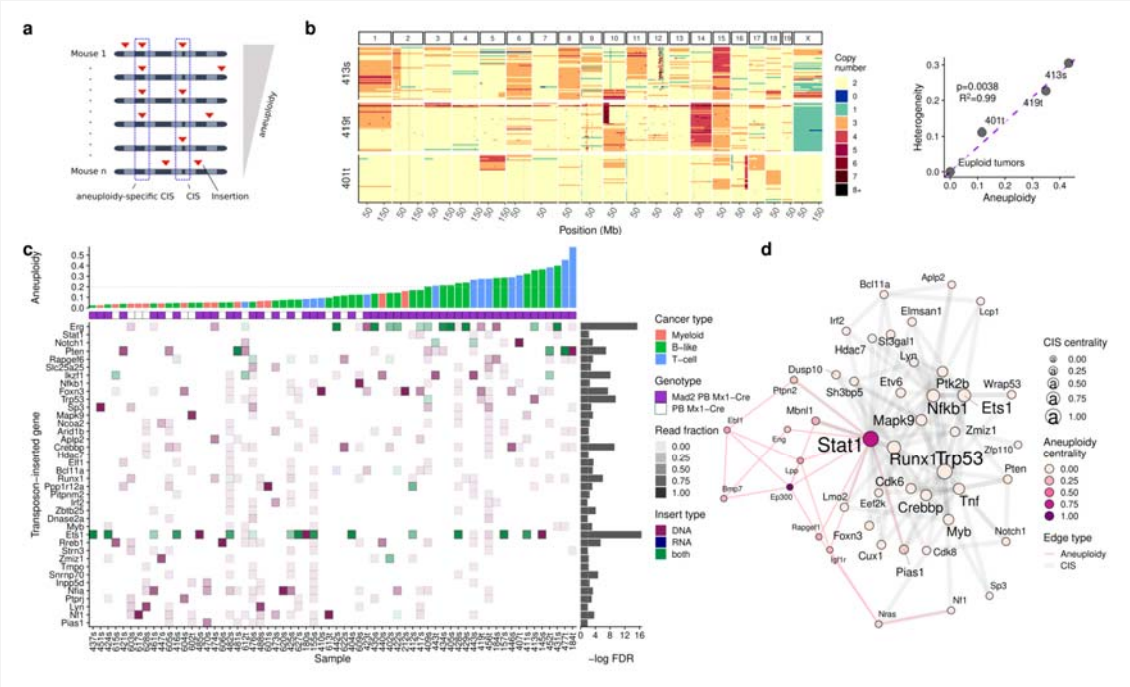

Fig. 2. Common Insertion Sites (CIS) in the mouse transposon cohort. **(a)** Schema of finding CIS that are occurring more than expected by chance, or in addition occurring more towards either end of the aneuploidy spectrum. **(b)** Single-cell whole genome sequencing of three tumors shows an almost-perfect correlation between aneuploidy and copy number heterogeneity, a measure of CIN. It is the basis of treating aneuploidy and chromosomal instability interchangeably in the analysis of our mouse cohort. **(c)** Overview of the CIS. Mice are ordered from the most euploid to most aneuploid from left to right, insertion sites from the most euploid to most aneuploid from bottom to top. The color indicates evidence for the insertion found from DNA or RNA, with the shade corresponding to the relative DNA read count number. *Ets1* and *Erg* are the strongest general CIS, with *Erg* and *Stat1* the most aneuploidy-enriched, and *Pias1* the most euploid-enriched. **(d)** Core of the merged insertion subnetwork of both general (grey lines) and aneuploidy-specific CIS (pink lines). *Trp53* is central in the general network, *Ep300* in the CIN network, and *Stat1* in both. All tests performed using a linear model unless stated otherwise.

To better understand the biology of the euploid and aneuploid malignancies, we next analyzed the transcriptomes of all tumors. We confirmed our earlier FACS-based cancer type classification with the gene expression of differentiation markers. Samples clustered according to their cancer type (**Fig. 3a**), and showed an upregulation of the respective lineage (**Fig. 3b, S3a**), *e.g.* CD3 for T-ALLs, Ebf1 for B-like precursors, and Ly6g (GR-1)/Lyz1 for myeloid malignancies. In addition, B-like precursors showed a higher expression of cKit, and a subset harbored an aberrant activation of the Ets1 or Erg transcription factors (B220 low in FACS; **Fig. S1c**), similar to a human leukemia cohort (**Fig. S3b**). Interestingly, the level of aneuploidy in our mouse cohort also reflects that in human pro/pre-B-ALL (Ebf1 and Ets1), and hyperdiploid ALL (Erg). T-ALLs and myeloid leukemias can be both euploid and aneuploid, although there is a bias for more aneuploid T-ALLs and more euploid myeloid leukemias in our mice compared to the human cohort (**Fig. S3c**).

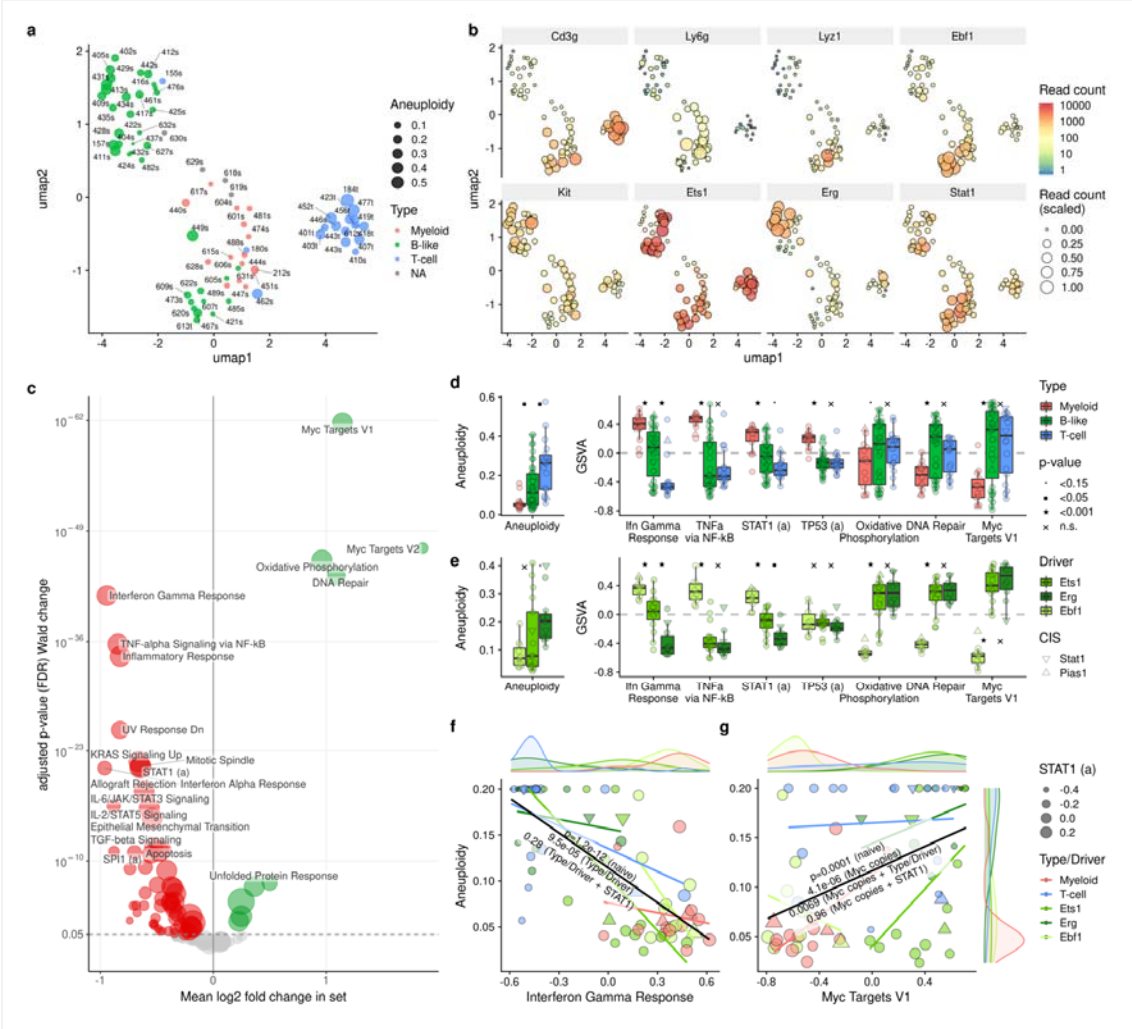

Fig. 3. Gene expression in the mouse transposon cohort. **(a)** Dimensionality reduction (UMAP) plot of the gene expression of known differentiation markers shows a distinct cluster for T-ALLs and Ets1/Erg-driven B-like tumors. Ebf1-driven B-like and myeloid tumors show a continuum, in agreement with the histiocytic sarcoma transdifferentiation identified by histology and FACS markers. **(b)** Gene expression of markers for the tumors shows expected expression of Cd3 and T-ALL, Ets1/Erg/Ebf1 in B-like, and Ly6g/Lyz in myeloid tumors. Kit expression is consistent with Ets1/Erg locking tumors in a precursor state that has low Stat1 expression, and Stat1 expression is consistent with baseline expression of the interferon response. **(c)** Differential expression with aneuploidy, corrected for tumor type, shows a downregulation of the Interferon Response and Stat1 target genes, and upregulation of the Myc Targets Hallmark gene set. Oxidative Phosphorylation and DNA repair sets are also upregulated. **(d)** Aneuploidy levels and gene set expression between tumors mirrors the effect observed within tumors, also **(e)** when splitting B-like tumors into its specific drivers. **(f)** Sample-level expression of the Interferon Gamma Response is strongly correlated with aneuploidy, which can be fully explained by tumor subtype in combination with Stat1 activity, but not subtype alone. **(g)** Myc targets positively correlate with aneuploidy, which can be explained by Myc DNA copies only in combination with Stat1 activity, but not by Myc copy number or subtype alone (parenthesis indicate covariate in regression). Boxplots show median and quartiles, whiskers the interquartile range. All tests performed using a linear model unless stated otherwise. Transcription factor activity inference indicated with uppercase letters and (a) for activity.

Next, we quantified which gene expression changes correlate with increased levels of aneuploidy or CIN in our cohort. While correcting for potential confounders of different cancer types, we find an overall strong signal for an inactivation of Stat1 and the interferon/inflammatory response, and an upregulation of Myc targets, with Oxidative Phosphorylation and DNA repair as second-line hits (**Fig. 3c**). The p53

response and the expression of p53 transcriptional targets were largely unchanged, in agreement with our observation that *Trp53* did not show preferential transposon insertions in either euploid or aneuploid tumors. If we, instead of correcting for different cancer types, use their respective gene set expression, we find that the observed differences mirror the different aneuploidy levels also across cancer types (**Fig. 3d**). Splitting our B-like cancer type into Ebf1, Ets1, and Erg-driven tumors, we again observe a consistent pattern between differential expression and aneuploidy/CIN levels (**Fig. 3e**).

While Stat1 is thought of as the primary driver for the interferon response (*40*), we have yet to show that this is true for our cohort. To do this, we inferred Stat1 activity from expression of its target genes, and tested whether this activity can fully explain the correlation between CIN and the expression of the interferon response gene set (**Fig. 3f**). Indeed, we find that when conditioning the association on the cancer type and Stat1 activity, this correlation drops from strongly significant to not significant, indicating that the interferon response is likely driven via Stat1. Similarly, we can show that the correlation between Myc targets and CIN can be explained by Myc copies in combination with Stat1 activity, but not by Myc copies alone or in combination with cancer type (**Fig. 3g**), indicating that Stat1 restricts Myc activity. We conclude that, in our model system, aneuploid hematopoietic malignancies inactivate inflammatory signaling through Stat1 inactivation. CIN, on the other hand, enables oncogene amplification, which in our model predominantly involved Myc. Stat1 inactivation in combination with higher Myc levels yield a high transcription level of Myc target genes.

Transformed 3T3 cells demonstrate Stat1-driven immune recruitment and immune cell activation in response to CIN

We next set out to validate whether our identified driver genes indeed promote malignant transformation of CIN cells *in vivo*. For this, we engineered an untransformed mouse fibroblast cell line (NIH/3T3) with the main factors that we identify to selectively drive tumors with a CIN phenotype (Myc overexpression with or without Stat1 inactivation). As a non-CIN specific control for transformation, we also engineered p53-deficient 3T3 cells with or without Stat1 (**Fig. 4a**, **Fig. S4a-c**). We chose 3T3 fibroblasts as they represent a very different tissue type and thus allow us to generalize our findings. Furthermore, 3T3 cells can be allografted in immuno-proficient mice to study the interaction of the engineered cancer cells with a fully functional immune environment. To induce chromosomal instability, we introduced dnMCAK, a mutant version of the tubulin-binding protein MCAK (also known as KIF2C) into all four 3T3 genotypes (Myc^{OEX} or $p53^{KO}$, each with or without Stat1). As a non-CIN control, we in parallel introduced wild type KIF2C (*41*) (**Fig. 4a**). CIN phenotypes were confirmed by time-lapse microscopy imaging (**Fig. S4d-f**) and caused a moderate proliferation increase for Myc^{OEX};$Stat1^{KO}$ and decrease for $p53^{KO}$, albeit not significantly (**Fig. 4b**).

Given the established roles of Stat1 and Myc in inflammation and immune attraction (*42–44*), we then quantified migration of $CD45^{+}$ immune cells (primary isolated Balb/c splenocytes) towards our engineered 3T3 genotypes in a trans-well assay. We find that dnMCAK-induced CIN promotes immune cell migration, and that this is mildly reduced upon overexpression of Myc, but not upon p53 loss. This migration is largely prevented by concomitant Stat1 inactivation in both Myc^{OEX} and $p53^{KO}$ cells (**Fig. 4c**), suggesting that Stat1 activity drives CIN-dependent immune cell infiltration. We next assessed anchorage independent growth as a readout for transformation, which confirmed that all eight engineered genotypes (**Fig. 4a**) grow in soft agar, unlike the parental cell line (**Fig. 4d**). While Myc^{OEX} cells formed large colonies irrespective of other genetic modifications, $p53^{KO}$ cells displayed inhibited growth with either CIN and $Stat1^{KO}$, or the combination thereof. We then inoculated immune-compromised mice with the engineered 3T3 cell lines and found that all cell lines formed tumors efficiently within 13-20 days. Myc^{OEX};KIF2C tumors showed a higher latency compared to either dnMCAK or $Stat1^{KO}$, with the combination being the most proliferative (**Fig. 4e**). By contrast, $p53^{KO}$;KIF2C were the fastest to grow

out, with a delay upon either CIN or Stat1^{KO} (**Fig. 4f**), in agreement with their *in vitro* growth characteristics.

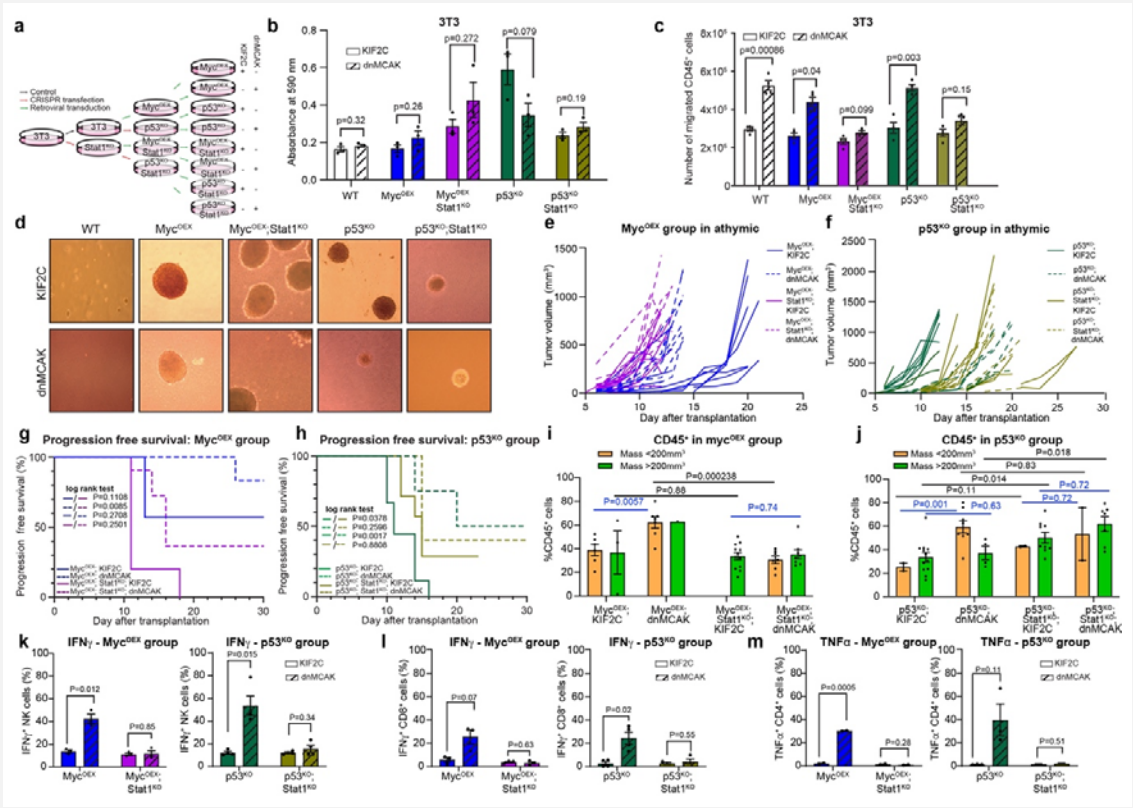

Fig. 4. Chromosomal instability promotes Stat1-mediated inflammatory signaling and immune recruitment. **(a)** Schematic overview depicting steps to generate genetically engineered 3T3 transformed lines. **(b)** Crystal violet assay showing the difference in the growth of the engineered 3T3 cell lines with KIF2C (CIN^{low}) and dnMCAK (CIN^{high}). **(c)** A transwell migration assay demonstrated increased immune cell attraction towards 3T3 cells with a CIN phenotype in a Stat1 proficient background. Inactivation of Stat1 attenuated this effect. **(d)** Representative images from 3T3 genotypes grown in soft agar as an *in vitro* readout of malignant transformation of the engineered 3T3 cell lines. **(e,f)** Inoculation of immunocompromised mice with the 3T3 engineered cell lines overexpressing Myc^{OEX} **(e)** or with a p53^{KO} background **(f)** shows similar growth kinetics *in vivo* compared to *in vitro* (see panel **b**) without a significant growth penalty imposed by CIN. **(g-h)** Progression free survival (tumor size < 500 mm^3) for tumor fragments allografted in both flanks of immunocompetent Balb/c mice from Myc^{OEX} **(g)** and p53^{KO} **(h)** 3T3 cell lines with or without Stat1 inactivation (n=8 mice per genotype). CIN increased tumor latency for Stat1 proficient tumors and Stat1 loss reduced tumor latency. **(i-j)** Quantification of the CD45$^+$ immune cell fraction by flow cytometry within the allograft tumors showed an increase in Myc^{OEX} **(i)** and p53^{KO} **(j)** tumors, which was rescued by Stat1 inactivation in Myc^{OEX} tumors, but not in p53^{KO} tumors. **(k-m)** Cytokine production measured by FACS as a readout of *ex vivo* immune cell activation in NK cells **(k)**, CD8$^+$ cells **(l)** or CD4$^+$ cells **(m)** co-cultured with Myc^{OEX} (left panels) and p53^{KO} 3T3 cells (right panels) reveals that 3T3 cells that display CIN activate each of these immune cell types and that Stat1 inactivation alleviates this. Error bars represent mean ± standard error of mean (s.e.m). **(b,d,i-m)** Significance tested using a two-sided t-test and **(g-h)** log rank test.

To determine the impact of a functional immune system on tumor development, we next allografted 3T3 tumor fragments into Balb/c mice and followed them during tumor progression. Unlike in immuno-compromised mice, we find that Myc^{OEX};dnMCAK cells do not show progressive tumor growth (**Fig. 4g, Fig. S5a**). This suggests that they proliferate efficiently themselves but are eliminated by a functional immune system. Concomitant Stat1^{KO} rescues this CIN-imposed growth delay and restores progressive tumor growth in these mice. By contrast, p53^{KO} tumors generally progress but show a significant delay

with dnMCAK compared to non-CIN cells (**Fig. 4h, Fig. S5b**). This difference is compensated by concomitant Stat1^{KO}, but these genotypes are still not as aggressive as p53^{KO};KIF2C.

We next quantified immune cell infiltration for all transplanted tumor fragments, including tumors that showed little to no growth (<200 mm^3). We find that dnMCAK-induced CIN promotes immune infiltration (*i.e.* the fraction of CD45$^+$ cells) in Myc^{OEX} tumors by ~50%, which is rescued by Stat1 loss (**Fig. 4i, Fig. S5d-e**). By contrast, in p53^{KO} tumors, dnMCAK and Stat1^{KO} tend to increase the fraction of CD45$^+$ cells, despite efficient outgrowth of these tumors (**Fig. 4j, Fig. S5d-e)**. These observations suggest that CIN impairs Myc^{OEX} tumor outgrowth by recruiting immune cells that Stat1 loss can rescue, while p53^{KO} tumors are less influenced by immune infiltration. Further characterization of the immune cell types in Stat1 proficient tumors revealed that dnMCAK-induced CIN increases the fraction of CD4$^+$, CD8$^+$, NK and CD19$^+$ cells within the CD45$^+$ population, particularly in tumors that showed little growth (<200 mm^3, **Fig. S5f-i**). Inactivation of Stat1 does not change the immune landscape drastically, except for decreasing the fraction of NK and CD19$^+$ cells in CIN-driven Myc^{OEX} tumors and decreasing the fraction of CD19$^+$ in p53^{KO} tumors (**Fig. S5f-i**). To determine the functional importance of the Stat1 loss-imposed alteration in the *in vivo* immune landscape, we isolated splenocytes from Balb/c mice and exposed them to all eight engineered 3T3 cell lines. We quantified immune cell activation by measuring IFNγ production for NK and CD8$^+$ cells and TNFα production for CD4$^+$ cells. We find, in agreement with work of others (*13*, *15*, *45*, *46*), that CIN activates NK, CD4$^+$, and CD8$^+$ cells. Furthermore, we find that Stat1 inactivation in the 3T3 cells alleviates this response, both in a Myc^{OEX} and p53^{KO} background (**Fig. 4k-m**). From these *ex vivo* experiments, we conclude that Stat1 is required to activate NK, CD4$^+$ and CD8$^+$ cells in tumors that display CIN.

Altogether, these data show that loss of Stat1 activity is required for the *in vivo* growth of Myc-driven tumors with a CIN phenotype. By contrast, p53-deficient tumors grow most efficiently in a non-CIN setting, irrespective of the presence of an immune system. Importantly, these findings functionally validate the significance of Stat1 inactivation from our transposon screen.

STAT1/MYC drive CIN tolerance in human cancer

Having shown that Myc activation necessitates Stat1 inactivation in chromosomally unstable mouse tumors, we were wondering if the same holds true in human cancers. For this, we took 11 TCGA cohorts for which a separate quantification of immune and stromal contamination was available (ESTIMATE algorithm, details methods). We quantified the expression change of both MYC target genes and STAT1 transcription factor target genes with aneuploidy, and found that most cancers activate MYC targets and inactivate STAT1 target genes (**Fig. 5a**). We further confirmed this by showing that aneuploid tumors show a higher fraction of STAT1 mutations than euploid tumors (**Fig. 5b**), in agreement with the transposon insertion data from our hematopoietic mouse tumors. However, STAT1 mutations only rarely occur in human cancers (2.3%), so there must be additional aberrations to explain the widespread inactivation we observed in our transcription factor activity inference (**Fig. 5a**). One such previously identified factor is a recurrent loss of the interferon alpha gene cluster on chromosome 9, often in combination with *CDKN2A* (*47*). Still, the combined prevalence of both alterations only amounts to 8% across human tumors. This difference may be explained by STAT1 interactor mutations in both our mouse cohort (**Fig. S2d**) and human cancers (**Fig. 5c**), but we need additional data to estimate the effect that each of these mutations may have.

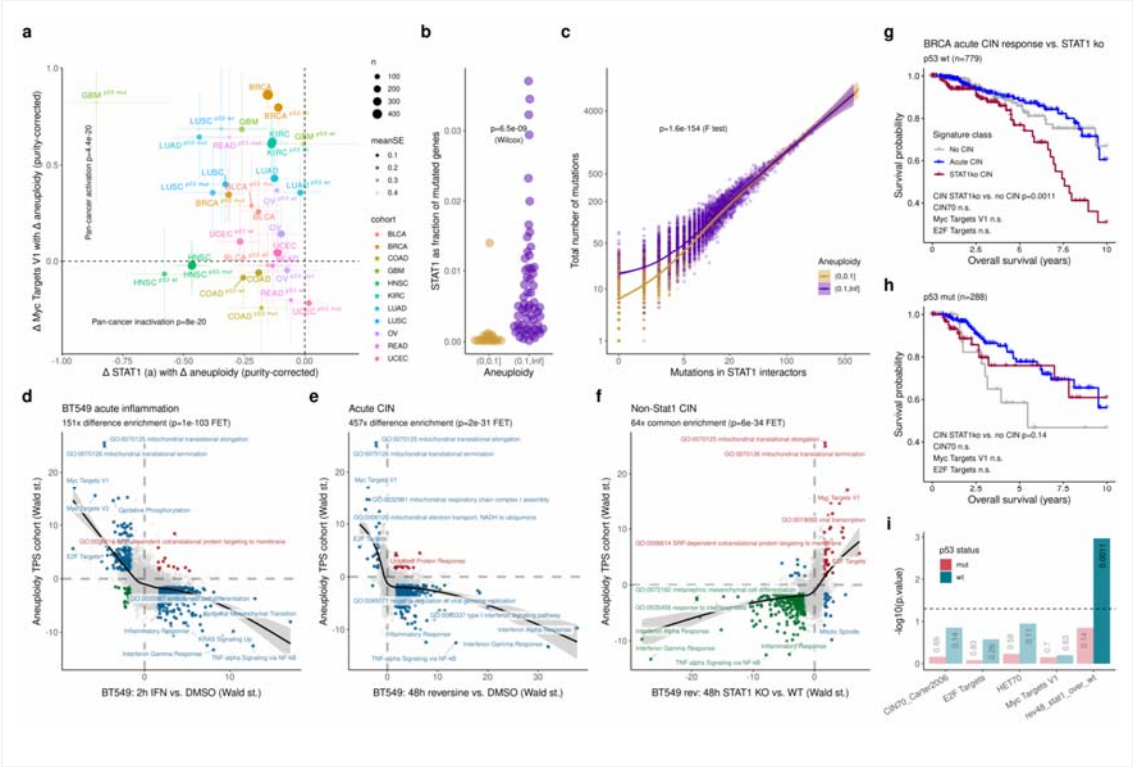

Fig. 5. STAT1 in human aneuploid cancer. **(a)** Across 11 TCGA cohorts, all show decrease of STAT1 target genes with increasing levels of aneuploidy when regressing out tumor purity. Myc targets are increased for most cohorts. *TP53* mutated and wild-type samples show the same trend. Bars represent standard error of the slope. **(b)** *STAT1* mutations make up a higher fraction of total mutations in aneuploid samples compared to euploid samples. **(c)** STAT1 interactor mutations make up a lower fraction of total mutations in aneuploid compared to euploid samples when the total mutation rate is low, consistent with transposon insertions. **(d)** Interferon and reversine **(e)** treatment of BT549 cells show the opposite gene expression difference to the CIN adaptation in our mouse transposon cohort for most gene sets in a merged collection of MSigDB Hallmarks, DoRothEA and Gene Ontology. **(f)** Reversine-treated BT549 cells with *STAT1* knockout compared to wild-type show very similar expression changes to CIN adaptation in the transposon cohort. FET Fisher's Exact Test of the four colored quadrants. **(g)** Cox Proportional Hazards model shows a difference in TCGA breast cancer 10-year overall patient survival when the STAT1^{ko} signature is present compared to when it is absent for p53 wild-type tumors, but not for p53-mutant tumors **(h)**. Alternative explanations like proliferation and CIN signatures show no significant difference **(i)**. Cox models regressed out age at diagnosis and tumor purity. All tests performed using a linear model unless stated otherwise.

In order to address this, we utilize gene expression changes upon STAT1 inactivation in a CIN setting. We chose the chromosomally stable BT549 breast cancer cell line to model a tissue with high MYC activation and on average only moderate STAT1 downregulation. We treated BT549 cells with either Type I interferon or reversine, an MPS1 inhibitor that induces CIN (**Fig. S6a**). RNA sequencing confirmed a transcriptional inflammatory response common to both treatments, and revealed an overall opposite effect compared to the acquired CIN tolerance in our mouse cohort (**Fig. 5d-e**). We then removed *STAT1* via CRISPR-mediated gene knockout and found that the gene expression changes in a CIN setting strongly mimicked the acquired CIN tolerance of our mouse cohort (**Fig. 5f**). Phenotypically, the knockout did not significantly alter proliferation or CIN (**Fig. S6b-d**), but did promote survival and decreased immune cell attraction and activation in response to CIN (**Fig. S6e-h**), consistent with another cell line (**Fig. S6i-m**) and our transformed mouse fibroblasts (**Fig. 4**). This suggests that STAT1 inactivation is a conserved mechanism for CIN tolerance across cell types and species.

Importantly, the latter experiment provided us with a tool to score STAT1 inactivation in a CIN setting across the TCGA breast cancer cohort independent of known markers such as a *STAT1* mutation or *IFNA* loss. We confirmed that our scores positively correlate with aneuploidy and previously published CIN signatures (**Fig. S7a**) as orthogonal measures of CIN. If they truly reflect CIN levels, we would expect them to also correlate with the clinical outcome of CIN, such as treatment response or metastasis formation. We hence divided the human breast cancer patients into CIN-low (no inflammation, no STAT1^{KO} expression signature), acute CIN (high inflammatory signature) and STAT1^{KO} CIN (no inflammation, STAT1^{KO} signature). Indeed, we observed a significant decrease in 10-year overall survival in the STAT1^{KO} patients compared to inflammatory CIN or no-CIN for *TP53* wild-type tumors (**Fig. 5g**). This difference was not present in *TP53* mutant tumors (**Fig. 5h**), and could neither be explained by proliferation (E2F targets), Myc target genes, or other available CIN signatures (**Fig. 5i**).

While it seems counterintuitive that p53-mutant tumors show a better patient survival effect when the STAT1^{KO} signature is present (**Fig. 5h**) contrary to p53 wild-type tumors (**Fig. 5g**), this observation is consistent with our 3T3 data. Murine p53-driven tumors (**Fig. 4j**) showed a higher immune infiltration than Myc-driven tumors (**Fig. 4i**), even when Stat1 was inactivated, and a delayed outgrowth in their primary host adaptation (**Fig. 4f**). As human STAT1^{KO} breast cancer p53 mutant tumors also show a higher immune infiltration than their p53 wild type counterparts (**Fig. S7b**), the better survival of patients with p53 mutant cancers without STAT1 signaling can be explained by an increased immune surveillance. This leads us to the conclusion that MYC activation co-operates with STAT1 inactivation for immune evasion across cancer types and species boundaries, where STAT1 inactivation allows for increased MYC target gene expression (**Fig. S7c**) that cannot be explained by alternate factors (**Fig. S7d**).

Discussion

We have presented an *in vivo* CIN screen that, from a common starting point of a genetically engineered mouse model, mirrored random gene activation or inactivation using genome-wide transposon insertional mutagenesis. The advantage of this approach is that it takes into account co-evolutionary trajectories between oncogene-driven carcinogenesis and the response of the immune system that is not modeled in the classic yeast or cell culture studies. Furthermore, the isogenic starting point offers controlled conditions with a limited number of potential external factors that may influence this process, unlike observational studies of a human cancer cohort. Owing to this, we can make a well-founded statement about the relative importance of different kinds of oncogenes in an engineered CIN *vs.* non-CIN setting.

A particularly interesting aspect of our findings is that, while p53 has often been described as the most obvious CIN-tolerating mutation, it seems to enable both euploid and CIN cancers approximately evenly. This effect is likely a combination of the fact that cell-intrinsically, both CIN and Stat1^{KO} reduce growth of p53^{KO} cells, whereas *in vivo* Stat1^{KO} prevents efficient immune activation (but not infiltration). The detrimental effect of CIN we observed in our mouse experiments is reflected in a human breast cancer cohort, where patients with *TP53* mutant tumors show the overall worst survival without CIN, the opposite of *TP53* wild-type tumors. *TP53* mutant tumors, however, still show on average higher levels of aneuploidy, likely reflecting an imperfect correlation between aneuploidy and CIN in observational cohorts like the TCGA.

Myc activation, on the other hand, seems to be CIN-specific, as evidenced by the recurrent copy number amplifications both in our mouse cohort and across different human cancers. Strikingly, the lack of transposon insertions in Myc, combined with the lack of transcriptional upregulation of MYC in human cancers above its amplification status (*50*), suggests that CIN is required exactly because it enables these copy number amplifications and MYC as an oncogene is inert to epigenetic modulation. Previously, MYC-driven cancers have been described to be immune exclusionary by matter of the protein itself.

Here, we find that with the pro-inflammatory effect of mis-segregations, cancer cells restrict Myc target transcription and will still be eliminated by both the innate (NK cells) and adaptive (T-cells) immune system. In order to overcome this, CIN-driven tumors need to dampen their interferon response, which they achieve through inactivation of Stat1 signaling. We showed that overexpression of the Myc oncogene and loss of Stat1 work synergistically in evading immune cells to sustain and promote the growth of CIN tumors in our mouse cohort and a clean engineered and allografted system in 3T3 cells, consistent with what we observe in human patient tumors.

We do not yet know how loss of STAT1 signaling is driven exactly in most cases, as mutations of *STAT1*, even in combination with *IFNA* loss, only account for a subset of tumors that were scored as STAT1-low by our gene expression signature. However, we can assume that alterations in other genes exist that mediate STAT1 inactivation, as evidenced by the striking insertion/mutation pattern in STAT1 interactors and the observed loss of inferred STAT1 activity. Indeed, it has been shown that for example Ras activation can counteract Myc-driven immunosurveillance (*48*). We believe this will be an important aspect of follow-up studies and a starting point to designing therapies targeted at cancer-intrinsic inflammation. This could be done for instance through reactivation of STAT1 or inhibition of specific interactors, likely in combination with immune checkpoint inhibitors (*49*).

Finally, our data set provides a plethora of additional oncogenic hits that we did not explicitly follow up on, and we hope it will hence serve as a valuable resource for the CIN and aneuploidy community.

Acknowledgements

We thank Michel Weij and Daryll Eichorn at the central animal facility for assistance with animal experiments and Johan Teunis and Theo Bijma at the flow cytometry facility for help with flow cytometry. We thank Rianna Arjaans and Nancy Halsema at the UMCG/ERIBA Research Sequencing facility for help with RNA sequencing library preparation and sequencing and Mathilde Broekhuis and Jonas Seiler at the UMCG/ERIBA iPSC/CRISPR facility for advice on the CRISPR KO experiments. We are grateful to Jiske Tiersma, Johanna Veldmann, Arthur Svendsen, Bertien Dethmers-Ausema, Maurits Roorda, Francien Talens and Chloe Lee for general advice on the project. We thank the members of the Foijer lab for fruitful discussions. This work was supported by Dutch Cancer Society Grants (2012-RUG-5549; 2015-RUG-7833 and 2018-RUG-11457) to Foijer, UMCG research fellowships to Hong and Requesens Rueda and a UMCG Cancer Research Fund (KRF) grant to Hong.

Author contributions

M.S., C.H., L.J.J., J.E.S. and F.F. conceived the project; M.S., C.H., L.J.J., M.R.R and F.F. designed the experiments; M.S. designed and performed all computational analyses and integrated all project data; L.J.J. and J.E.S. performed the transposon mutagenesis screen and harvested tumors with help of B.B and P.L.B.; M.H.K. and A.d.B. performed mouse pathology; J.L.C, A.D. and A.S. prepared samples for transposon integration analysis with help of J.E.S.; M.S., M.B., T.E. and H.P. mapped transposon integration sites; C.H., L.J.J., A.E.T, P.L.B, A.v.d.B, L.A.R, S.G., and D.L. performed *in vitro* experiments; D.C.J.S. supervised RNA, mini-bulk and scWGS sequencing. C.H. and M.R.R performed *in vivo* transplantation experiments, *ex vivo* immune assays and immune characterization of the transplanted tumors; H.W.N and M.d.B. co-supervised M.R.R; G.d.H. contributed reagents and supervised D.L.; R.H.M. and M.C.T. co-supervised M.S.; R.R. contributed reagents and supervised A.S. and M.B.; G.S.V. supervised J.L.C. and A.D., provided reagents and supervised transposon integration sequencing. M.S. C.H. and F.F. wrote the manuscript with input from M.R.R., M.A.T.M.v.V, M.C.T. and G.C.V; All authors reviewed and approved the manuscript.

Competing Interests

M.A.T.M.v.V. has acted on the Scientific Advisory Board of Repare Therapeutics, which is unrelated to this work. The other authors declare no conflict of interest.

References

1. K. M. Schukken, F. Foijer, CIN and Aneuploidy: Different Concepts, Different Consequences. *Bioessays.* **40** (2018), doi:10.1002/bies.201700147.

2. S. F. Bakhoum, B. Ngo, A. M. Laughney, J.-A. Cavallo, C. J. Murphy, P. Ly, P. Shah, R. K. Sriram, T. B. K. Watkins, N. K. Taunk, M. Duran, C. Pauli, C. Shaw, K. Chadalavada, V. K. Rajasekhar, G. Genovese, S. Venkatesan, N. J. Birkbak, N. McGranahan, M. Lundquist, Q. LaPlant, J. H. Healey, O. Elemento, C. H. Chung, N. Y. Lee, M. Imielenski, G. Nanjangud, D. Pe'er, D. W. Cleveland, S. N. Powell, J. Lammerding, C. Swanton, L. C. Cantley, Chromosomal instability drives metastasis through a cytosolic DNA response. *Nature.* **553**, 467–472 (2018).

3. U. Ben-David, A. Amon, Context is everything: aneuploidy in cancer. *Nat. Rev. Genet.* **21**, 44–62 (2020).

4. S. Santaguida, A. Amon, Short- and long-term effects of chromosome mis-segregation and aneuploidy. *Nat. Rev. Mol. Cell Biol.* **16**, 473–485 (2015).

5. S. Stingele, G. Stoehr, K. Peplowska, J. Cox, M. Mann, Z. Storchova, Global analysis of genome, transcriptome and proteome reveals the response to aneuploidy in human cells. *Mol. Syst. Biol.* **8**, 608 (2012).

6. G. A. Andriani, V. P. Almeida, F. Faggioli, M. Mauro, W. L. Tsai, L. Santambrogio, A. Maslov, M. Gadina, J. Campisi, J. Vijg, C. Montagna, Whole Chromosome Instability induces senescence and promotes SASP. *Sci. Rep.* **6**, 35218 (2016).

7. E. M. Torres, T. Sokolsky, C. M. Tucker, L. Y. Chan, M. Boselli, M. J. Dunham, A. Amon, Effects of aneuploidy on cellular physiology and cell division in haploid yeast. *Science.* **317**, 916–924 (2007).

8. B. R. Williams, V. R. Prabhu, K. E. Hunter, C. M. Glazier, C. A. Whittaker, D. E. Housman, A. Amon, Aneuploidy affects proliferation and spontaneous immortalization in mammalian cells. *Science.* **322**, 703–709 (2008).

9. J. M. Sheltzer, A. Amon, The aneuploidy paradox: costs and benefits of an incorrect karyotype. *Trends Genet.* **27**, 446–453 (2011).

10. A. Ohashi, M. Ohori, K. Iwai, Y. Nakayama, T. Nambu, D. Morishita, T. Kawamoto, M. Miyamoto, T. Hirayama, M. Okaniwa, H. Banno, T. Ishikawa, H. Kandori, K. Iwata, Aneuploidy generates proteotoxic stress and DNA damage concurrently with p53-mediated post-mitotic apoptosis in SAC-impaired cells. *Nat. Commun.* **6**, 7668 (2015).

11. F. Foijer, T. DiTommaso, G. Donati, K. Hautaviita, S. Z. Xie, E. Heath, I. Smyth, F. M. Watt, P. K. Sorger, A. Bradley, Spindle checkpoint deficiency is tolerated by murine epidermal cells but not hair follicle stem cells. *Proc. Natl. Acad. Sci. U. S. A.* **110**, 2928–2933 (2013).

12. F. Foijer, S. Z. Xie, J. E. Simon, P. L. Bakker, N. Conte, S. H. Davis, E. Kregel, J. Jonkers, A. Bradley, P. K. Sorger, Chromosome instability induced by Mps1 and p53 mutation generates aggressive lymphomas exhibiting aneuploidy-induced stress. *Proc. Natl. Acad. Sci. U. S. A.* **111**, 13427–13432 (2014).

13. S. Santaguida, A. Richardson, D. R. Iyer, O. M'Saad, L. Zasadil, K. A. Knouse, Y. L. Wong, N. Rhind, A. Desai, A. Amon, Chromosome Mis-segregation Generates Cell-Cycle-Arrested Cells with

Complex Karyotypes that Are Eliminated by the Immune System. *Dev. Cell.* **41**, 638–651.e5 (2017).

14. L. Senovilla, I. Vitale, I. Martins, M. Tailler, C. Pailleret, M. Michaud, L. Galluzzi, S. Adjemian, O. Kepp, M. Niso-Santano, S. Shen, G. Mariño, A. Criollo, A. Boilève, B. Job, S. Ladoire, F. Ghiringhelli, A. Sistigu, T. Yamazaki, S. Rello-Varona, C. Locher, V. Poirier-Colame, M. Talbot, A. Valent, F. Berardinelli, A. Antoccia, F. Ciccosanti, G. M. Fimia, M. Piacentini, A. Fueyo, N. L. Messina, M. Li, C. J. Chan, V. Sigl, G. Pourcher, C. Ruckenstuhl, D. Carmona-Gutierrez, V. Lazar, J. M. Penninger, F. Madeo, C. López-Otín, M. J. Smyth, L. Zitvogel, M. Castedo, G. Kroemer, An immunosurveillance mechanism controls cancer cell ploidy. *Science.* **337**, 1678–1684 (2012).

15. R. W. Wang, S. Viganò, U. Ben-David, A. Amon, S. Santaguida, Aneuploid senescent cells activate NF-κB to promote their immune clearance by NK cells. *EMBO Rep.* **22**, e52032 (2021).

16. E. Engidawork, G. Lubec, Protein expression in Down syndrome brain. *Amino Acids.* **21**, 331–361 (2001).

17. S. E. Dodgson, S. Santaguida, S. Kim, J. Sheltzer, A. Amon, The pleiotropic deubiquitinase Ubp3 confers aneuploidy tolerance. *Genes Dev.* **30**, 2259–2271 (2016).

18. J. E. Simon, B. Bakker, F. Foijer, CINcere Modelling: What Have Mouse Models for Chromosome Instability Taught Us? *Recent Results Cancer Res.* **200**, 39–60 (2015).

19. A. Vasudevan, K. M. Schukken, E. L. Sausville, V. Girish, O. A. Adebambo, J. M. Sheltzer, Aneuploidy as a promoter and suppressor of malignant growth. *Nat. Rev. Cancer* (2021), doi:10.1038/s41568-020-00321-1.

20. T. Fujiwara, M. Bandi, M. Nitta, E. V. Ivanova, R. T. Bronson, D. Pellman, Cytokinesis failure generating tetraploids promotes tumorigenesis in p53-null cells. *Nature.* **437**, 1043–1047 (2005).

21. D. J. Baker, F. Jin, K. B. Jeganathan, J. M. van Deursen, Whole chromosome instability caused by Bub1 insufficiency drives tumorigenesis through tumor suppressor gene loss of heterozygosity. *Cancer Cell.* **16**, 475–486 (2009).

22. F. Foijer, L. A. Albacker, B. Bakker, D. C. Spierings, Y. Yue, S. Z. Xie, S. Davis, A. Lutum-Jehle, D. Takemoto, B. Hare, B. Furey, R. T. Bronson, P. M. Lansdorp, A. Bradley, P. K. Sorger, Deletion of the MAD2L1 spindle assembly checkpoint gene is tolerated in mouse models of acute T-cell lymphoma and hepatocellular carcinoma. *Elife.* **6** (2017), doi:10.7554/eLife.20873.

23. M. Soto, J. A. Raaijmakers, B. Bakker, D. C. J. Spierings, P. M. Lansdorp, F. Foijer, R. H. Medema, p53 Prohibits Propagation of Chromosome Segregation Errors that Produce Structural Aneuploidies. *Cell Rep.* **19**, 2423–2431 (2017).

24. A. Narkar, B. A. Johnson, P. Bharne, J. Zhu, V. Padmanaban, D. Biswas, A. Fraser, P. A. Iglesias, A. J. Ewald, R. Li, On the role of p53 in the cellular response to aneuploidy. *Cell Rep.* **34**, 108892 (2021).

25. A. M. Taylor, J. Shih, G. Ha, G. F. Gao, X. Zhang, A. C. Berger, S. E. Schumacher, C. Wang, H. Hu, J. Liu, A. J. Lazar, Cancer Genome Atlas Research Network, A. D. Cherniack, R. Beroukhim, M. Meyerson, Genomic and Functional Approaches to Understanding Cancer Aneuploidy. *Cancer Cell.* **33**, 676–689.e3 (2018).

26. T. Davoli, H. Uno, E. C. Wooten, S. J. Elledge, Tumor aneuploidy correlates with markers of immune evasion and with reduced response to immunotherapy. *Science.* **355** (2017), doi:10.1126/science.aaf8399.

27. S. L. Carter, A. C. Eklund, I. S. Kohane, L. N. Harris, Z. Szallasi, A signature of chromosomal instability inferred from gene expression profiles predicts clinical outcome in multiple human cancers. *Nat. Genet.* **38**, 1043–1048 (2006).

28. J. M. Sheltzer, A transcriptional and metabolic signature of primary aneuploidy is present in chromosomally unstable cancer cells and informs clinical prognosis. *Cancer Res.* **73**, 6401–6412 (2013).

29. C. Buccitelli, L. Salgueiro, K. Rowald, R. Sotillo, B. R. Mardin, J. O. Korbel, Pan-cancer analysis distinguishes transcriptional changes of aneuploidy from proliferation. *Genome Res.* **27**, 501–511 (2017).

30. R. Rosenthal, E. L. Cadieux, R. Salgado, M. A. Bakir, D. A. Moore, C. T. Hiley, T. Lund, M. Tanić, J. L. Reading, K. Joshi, J. Y. Henry, E. Ghorani, G. A. Wilson, N. J. Birkbak, M. Jamal-Hanjani, S. Veeriah, Z. Szallasi, S. Loi, M. D. Hellmann, A. Feber, B. Chain, J. Herrero, S. A. Quezada, J. Demeulemeester, P. Van Loo, S. Beck, N. McGranahan, C. Swanton, C. Swanton, M. Jamal-Hanjani, S. Veeriah, J. Czyzewska-Khan, D. Johnson, J. Laycock, R. Rosenthal, P. Gorman, R. E. Hynds, G. Wilson, N. J. Birkbak, T. B. K. Watkins, N. McGranahan, M. Escudero, A. Stewart, P. Van Loo, A. Rowan, C. Hiley, C. Abbosh, J. Goldman, R. K. Stone, T. Denner, S. Ward, E. Nye, K. Joshi, A. Ben Aissa, Y. N. S. Wong, A. Georgiou, S. Quezada, J. A. Hartley, H. L. Lowe, J. Herrero, D. Lawrence, M. Hayward, N. Panagiotopoulos, M. Falzon, E. Borg, T. Marafioti, S. M. Janes, M. Forster, T. Ahmad, S. M. Lee, D. Papadatos-Pastos, D. Carnell, R. Mendes, J. George, A. Ahmed, M. Taylor, J. Choudhary, Y. Summers, R. Califano, P. Taylor, R. Shah, P. Krysiak, K. Rammohan, E. Fontaine, R. Booton, M. Evison, P. Crosbie, S. Moss, L. Joseph, P. Bishop, A. M. Quinn, H. Doran, A. Leek, P. Harrison, K. Moore, R. Waddington, J. Novasio, F. Blackhall, J. Rogan, E. Smith, C. Dive, J. Tugwood, G. Brady, D. G. Rothwell, J. Pierce, S. Gulati, B. Naidu, G. Langman, S. Trotter, H. Bancroft, A. Kerr, S. Kadiri, G. Middleton, M. Djearaman, D. Fennell, J. A. Shaw, J. Le Quesne, D. A. Moore, A. Nakas, S. Rathinam, W. Monteiro, H. Marshall, L. Nelson, J. Riley, L. Primrose, L. Martinson, G. Anand, S. Khan, M. Nicolson, K. Kerr, S. Palmer, H. Remmen, J. Miller, K. Buchan, M. Chetty, L. Gomersall, J. Lester, F. Morgan, H. Adams, H. Davies, M. Kornaszewska, R. Attanoos, S. Lock, M. MacKenzie, M. Wilcox, H. Bell, A. Hackshaw, Y. Ngai, S. Smith, N. Gower, C. Ottensmeier, S. Chee, B. Johnson, A. Alzetani, E. Shaw, E. Lim, P. De Sousa, M. T. Barbosa, A. Bowman, S. Jordan, A. Rice, H. Raubenheimer, H. Bhayani, M. Hamilton, N. Mensah, L. Ambrose, A. Devaraj, H. Chavan, A. G. Nicholson, K. Lau, M. Sheaff, P. Schmid, J. Conibear, V. Ezhil, V. Prakash, P. Russell, T. Light, T. Horey, S. Danson, J. Bury, J. Edwards, J. Hill, S. Matthews, Y. Kitsanta, K. Suvarna, P. Fisher, M. Shackcloth, J. Gosney, S. Feeney, J. Asante-Siaw, K. Ryanna, A. Dawson, M. Tuffail, A. Bajaj, J. Brozik, H. Walter, N. Carey, G. Price, K. Gilbert, J. Webb, A. Patel, A. Chaturvedi, F. Granato, K. Baker, M. Carter, L. Priest, M. G. Krebs, C. Lindsay, F. Gomes, F. Chemie, R. George, D. Patrini, R. Khiroya, P. Shaw, M. Skrzypski, M. W. Sunderland, J. L. Reading, C. Beastall, N. Mangal, K. Peggs, E. Lim, M. Al-Bakir, N. Navani, M. Scarci, L. Ensell, D. Biswas, R. Salgado, M. Razaq, J. Nicod, S. Beck, S. Lopez, A. Huebner, M. Dietzen, T. Mourikis, T. Adefila-Ideozu, S. Begum, H. Klein, A. Mani, S. Carvalho, D. Kaniu, C. Realingo, M. Malima, S. Booth, L. Lim, J. Rao, S. Tenconi, L. Socci, F. Kibutu, M. Agyemang, R. Young, K. G. Blyth, C. Dick, A. Kirk, A. Kidd, The TRACERx consortium, Neoantigen-directed immune escape in lung cancer evolution. *Nature* (2019), doi:10.1038/s41586-019-1032-7.

31. T. B. K. Watkins, E. L. Lim, M. Petkovic, S. Elizalde, N. J. Birkbak, G. A. Wilson, D. A. Moore, E. Grönroos, A. Rowan, S. M. Dewhurst, J. Demeulemeester, S. C. Dentro, S. Horswell, L. Au, K. Haase, M. Escudero, R. Rosenthal, M. A. Bakir, H. Xu, K. Litchfield, W. T. Lu, T. P. Mourikis, M. Dietzen, L. Spain, G. D. Cresswell, D. Biswas, P. Lamy, I. Nordentoft, K. Harbst, F. Castro-Giner, L. R. Yates, F. Caramia, F. Jaulin, C. Vicier, I. P. M. Tomlinson, P. K. Brastianos, R. J. Cho, B. C. Bastian, L. Dyrskjøt, G. B. Jönsson, P. Savas, S. Loi, P. J. Campbell, F. Andre, N. M. Luscombe, N. Steeghs, V. C. G. Tjan-Heijnen, Z. Szallasi, S. Turajlic, M. Jamal-Hanjani, P. Van Loo, S. F. Bakhoum, R. F. Schwarz, N. McGranahan, C. Swanton, Pervasive chromosomal instability and karyotype order in tumour evolution. *Nature* (2020), doi:10.1038/s41586-020-2698-6.

32. W. H. M. Hoevenaar, A. Janssen, A. I. Quirindongo, H. Ma, S. J. Klaasen, A. Teixeira, B. van Gerwen, N. Lansu, F. H. M. Morsink, G. J. A. Offerhaus, R. H. Medema, G. J. P. L. Kops, N. Jelluma, Degree and site of chromosomal instability define its oncogenic potential. *Nat. Commun.* **11**, 1501 (2020).

33. R. Sotillo, E. Hernando, E. Díaz-Rodríguez, J. Teruya-Feldstein, C. Cordón-Cardo, S. W. Lowe, R. Benezra, Mad2 overexpression promotes aneuploidy and tumorigenesis in mice. *Cancer Cell.* **11**, 9–23 (2007).

34. G. S. Vassiliou, J. L. Cooper, R. Rad, J. Li, S. Rice, A. Uren, L. Rad, P. Ellis, R. Andrews, R. Banerjee, C. Grove, W. Wang, P. Liu, P. Wright, M. Arends, A. Bradley, Mutant nucleophosmin and cooperating pathways drive leukemia initiation and progression in mice. *Nat. Genet.* **43**, 470–475 (2011).

35. R. Rad, L. Rad, W. Wang, J. Cadinanos, G. Vassiliou, S. Rice, L. S. Campos, K. Yusa, R. Banerjee, M. A. Li, J. de la Rosa, A. Strong, D. Lu, P. Ellis, N. Conte, F. T. Yang, P. Liu, A. Bradley, PiggyBac transposon mutagenesis: a tool for cancer gene discovery in mice. *Science.* **330**, 1104–1107 (2010).

36. Mitelman, F, Mitelman Database of Chromosome Aberrations and Gene Fusions in Cancer (2010), (available at http://cgap.nci.nih.gov/Chromosomes/Mitelman).

37. L. M. Sack, T. Davoli, M. Z. Li, Y. Li, Q. Xu, K. Naxerova, E. C. Wooten, R. J. Bernardi, T. D. Martin, T. Chen, Y. Leng, A. C. Liang, K. A. Scorsone, T. F. Westbrook, K.-K. Wong, S. J. Elledge, Profound Tissue Specificity in Proliferation Control Underlies Cancer Drivers and Aneuploidy Patterns. *Cell.* **173**, 499–514.e23 (2018).

38. T. Haferlach, A. Kohlmann, L. Wieczorek, G. Basso, G. T. Kronnie, M.-C. Béné, J. De Vos, J. M. Hernández, W.-K. Hofmann, K. I. Mills, A. Gilkes, S. Chiaretti, S. A. Shurtleff, T. J. Kipps, L. Z. Rassenti, A. E. Yeoh, P. R. Papenhausen, W.-M. Liu, P. M. Williams, R. Foà, Clinical utility of microarray-based gene expression profiling in the diagnosis and subclassification of leukemia: report from the International Microarray Innovations in Leukemia Study Group. *J. Clin. Oncol.* **28**, 2529–2537 (2010).

39. B. Liu, J. Liao, X. Rao, S. A. Kushner, C. D. Chung, D. D. Chang, K. Shuai, Inhibition of Stat1-mediated gene activation by PIAS1. *Proc. Natl. Acad. Sci. U. S. A.* **95**, 10626–10631 (1998).

40. M. A. Meraz, J. M. White, K. C. Sheehan, E. A. Bach, S. J. Rodig, A. S. Dighe, D. H. Kaplan, J. K. Riley, A. C. Greenlund, D. Campbell, K. Carver-Moore, R. N. DuBois, R. Clark, M. Aguet, R. D. Schreiber, Targeted disruption of the Stat1 gene in mice reveals unexpected physiologic specificity in the JAK-STAT signaling pathway. *Cell.* **84**, 431–442 (1996).

41. S. F. Bakhoum, S. L. Thompson, A. L. Manning, D. A. Compton, Genome stability is ensured by temporal control of kinetochore-microtubule dynamics. *Nat. Cell Biol.* **11**, 27–35 (2009).

42. N. Muthalagu, T. Monteverde, X. Raffo-Iraolagoitia, R. Wiesheu, D. Whyte, A. Hedley, S. Laing, B. Kruspig, R. Upstill-Goddard, R. Shaw, S. Neidler, C. Rink, S. A. Karim, K. Gyuraszova, C. Nixon, W. Clark, A. V. Biankin, L. M. Carlin, S. B. Coffelt, O. J. Sansom, J. P. Morton, D. J. Murphy, Repression of the Type I Interferon Pathway Underlies MYC- and KRAS-Dependent Evasion of NK and B Cells in Pancreatic Ductal Adenocarcinoma. *Cancer Discov.* **10**, 872–887 (2020).

43. C. V. Ramana, N. Grammatikakis, M. Chernov, H. Nguyen, K. C. Goh, B. R. Williams, G. R. Stark, Regulation of c-myc expression by IFN-gamma through Stat1-dependent and -independent pathways. *EMBO J.* **19**, 263–272 (2000).

44. S. Swaminathan, A. S. Hansen, L. D. Heftdal, R. Dhanasekaran, A. Deutzmann, W. D. M. Fernandez, D. F. Liefwalker, C. Horton, A. Mosley, M. Liebersbach, H. T. Maecker, D. W. Felsher, MYC functions as a switch for natural killer cell-mediated immune surveillance of lymphoid malignancies. *Nat. Commun.* **11**, 2860 (2020).

45. A. Acebes-Huerta, S. Lorenzo-Herrero, A. R. Folgueras, L. Huergo-Zapico, C. Lopez-Larrea, A. López-Soto, S. Gonzalez, Drug-induced hyperploidy stimulates an antitumor NK cell response mediated by NKG2D and DNAM-1 receptors. *Oncoimmunology.* **5**, e1074378 (2016).

46. F. Aranda, K. Chaba, N. Bloy, P. Garcia, C. Bordenave, I. Martins, G. Stoll, A. Tesniere, G. Kroemer, L. Senovilla, Immune effectors responsible for the elimination of hyperploid cancer cells. *Oncoimmunology.* **7**, e1463947 (2018).

47. S. F. Bakhoum, L. C. Cantley, The Multifaceted Role of Chromosomal Instability in Cancer and Its Microenvironment. *Cell.* **174**, 1347–1360 (2018).

48. R. M. Kortlever, N. M. Sodir, C. H. Wilson, D. L. Burkhart, L. Pellegrinet, L. Brown Swigart, T. D. Littlewood, G. I. Evan, Myc Cooperates with Ras by Programming Inflammation and Immune Suppression. *Cell.* **171**, 1301–1315.e14 (2017).

49. S. C. Casey, L. Tong, Y. Li, R. Do, S. Walz, K. N. Fitzgerald, A. M. Gouw, V. Baylot, I. Gütgemann, M. Eilers, D. W. Felsher, MYC regulates the antitumor immune response through CD47 and PD-L1. *Science.* **352**, 227–231 (2016).

50. K. M. Schukken, J. M. Sheltzer, Extensive protein dosage compensation in aneuploid human cancers. *bioRxiv* (2021), p. 2021.06.18.449005.

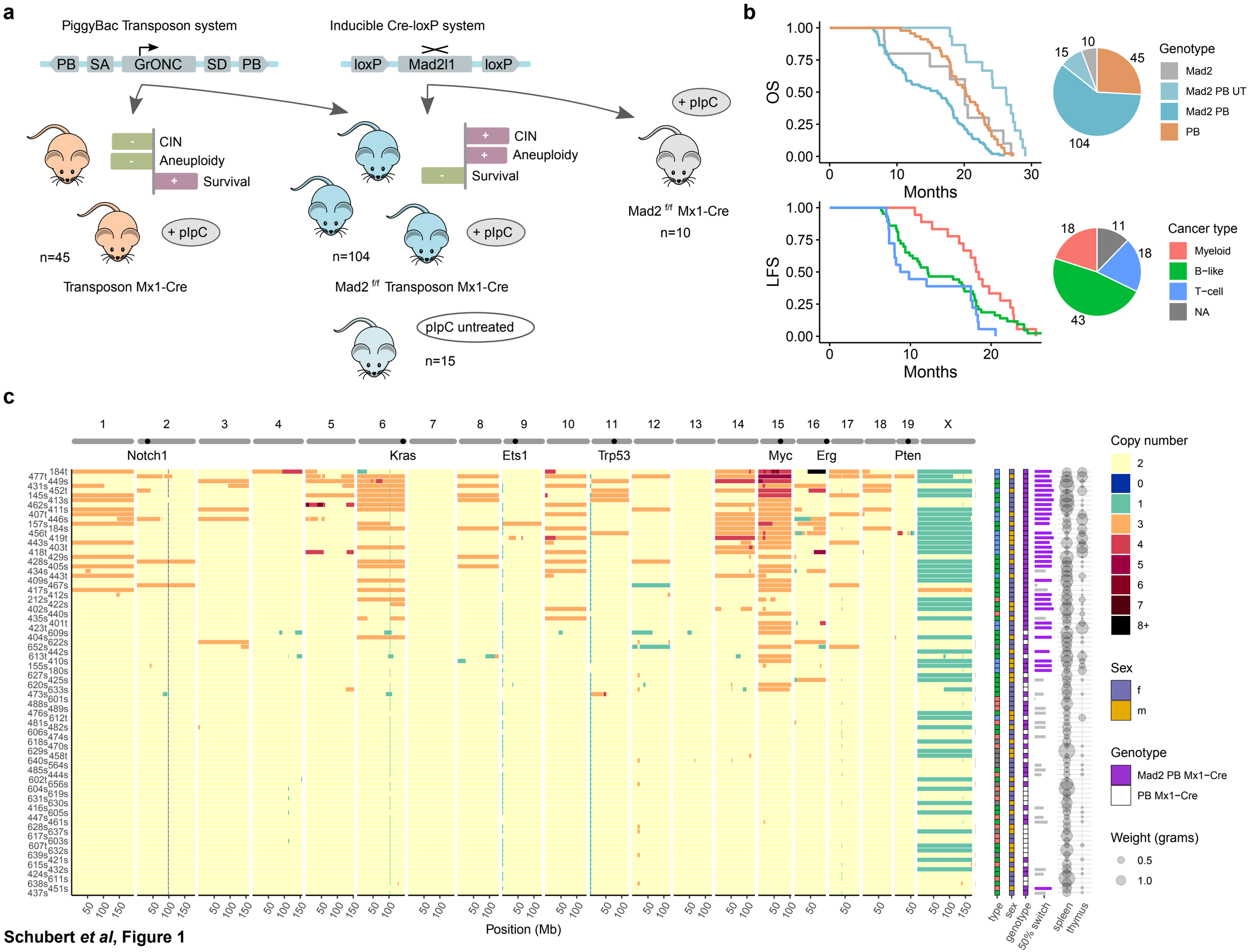

Schubert *et al*, Figure 1

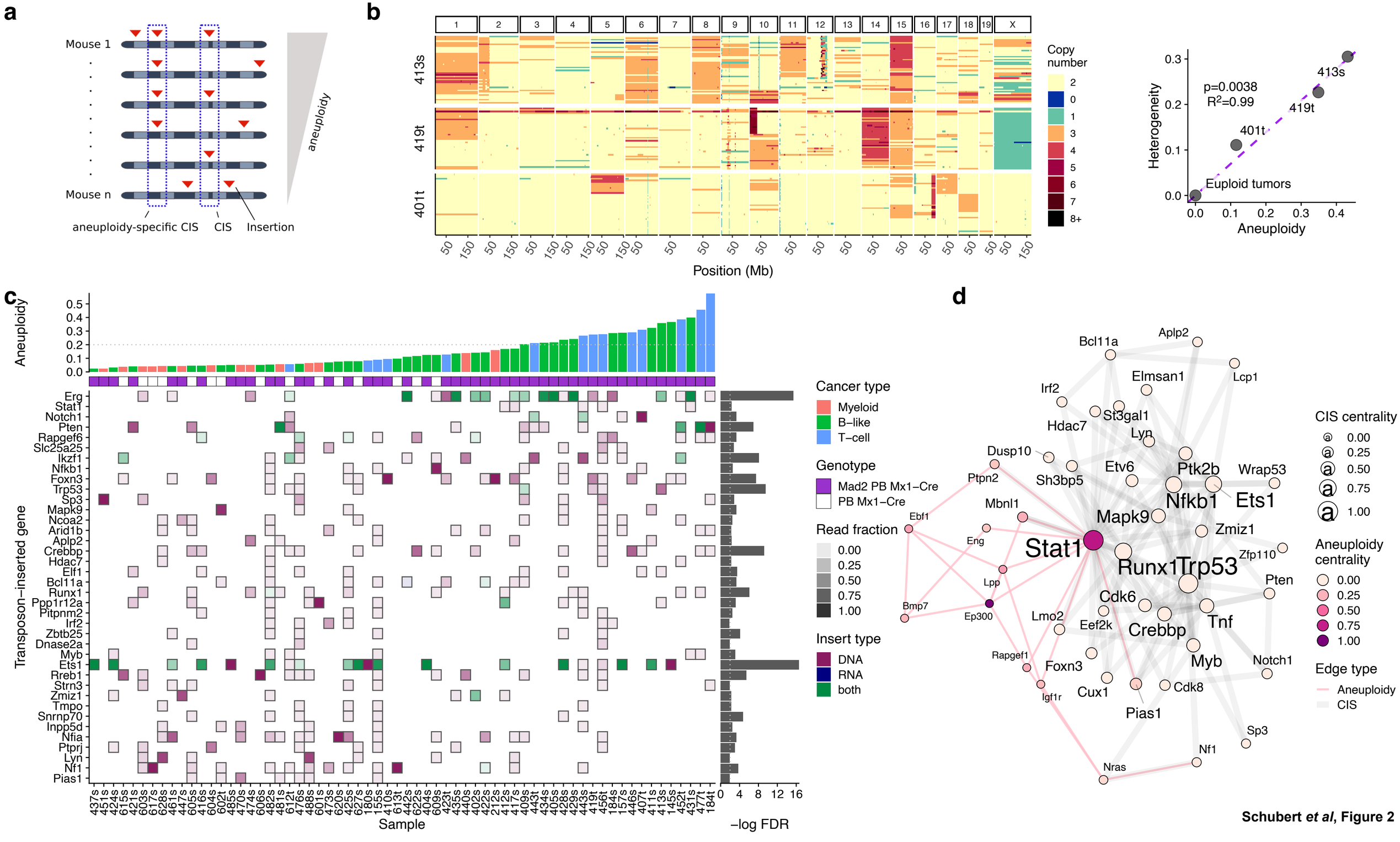

Schubert *et al*, Figure 2

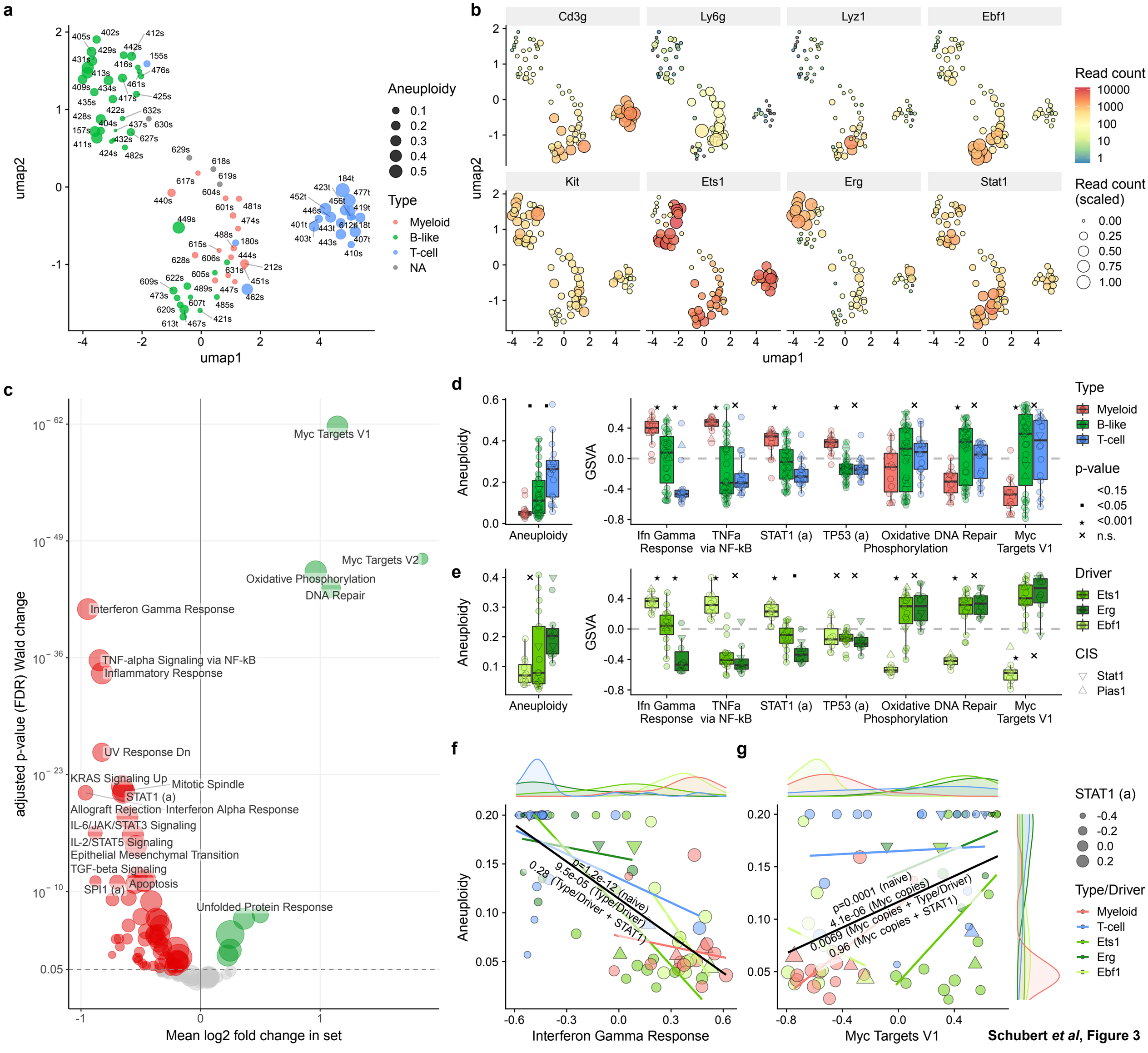

Schubert *et al*, Figure 3

Schubert *et al*, Figure 4

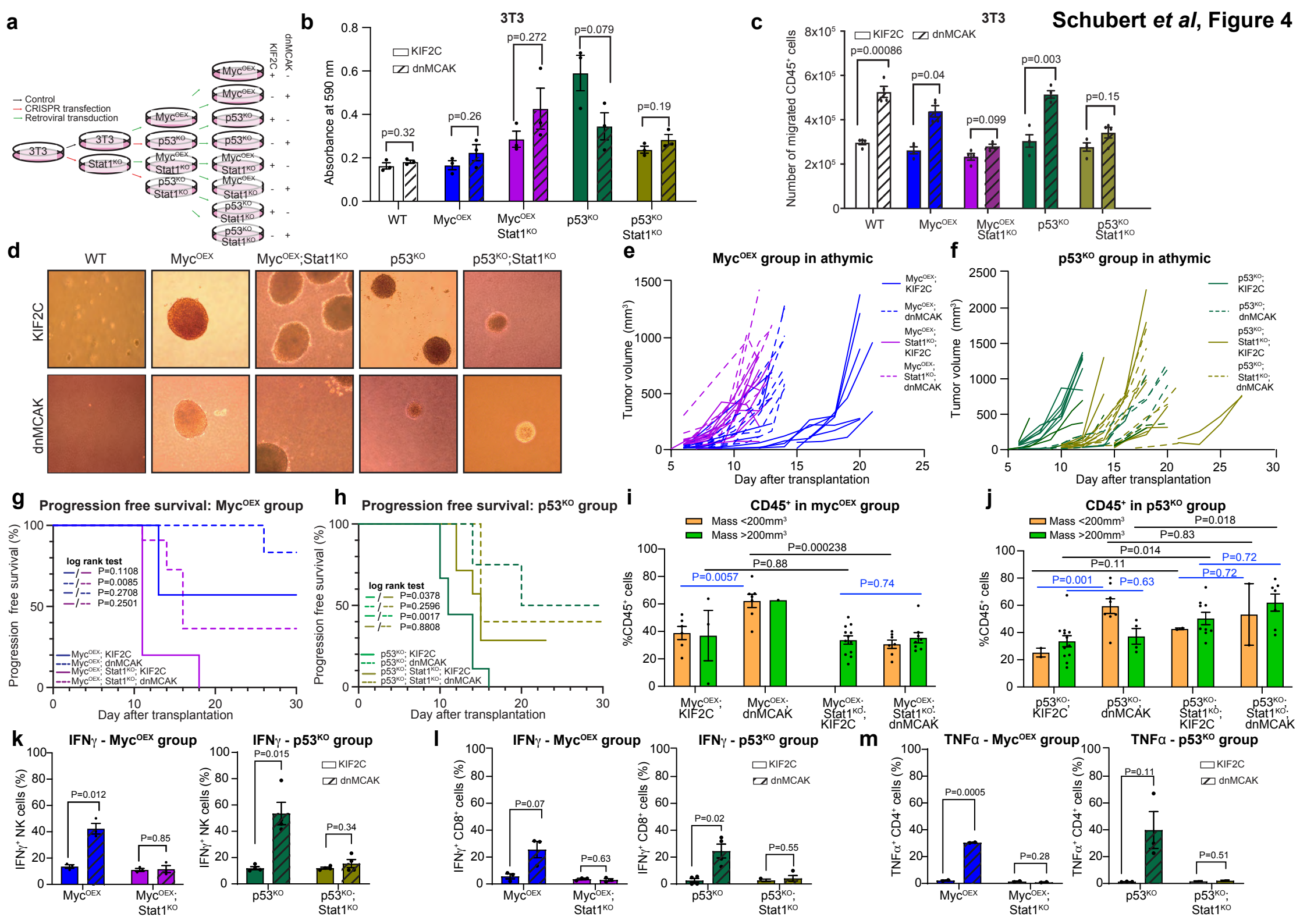

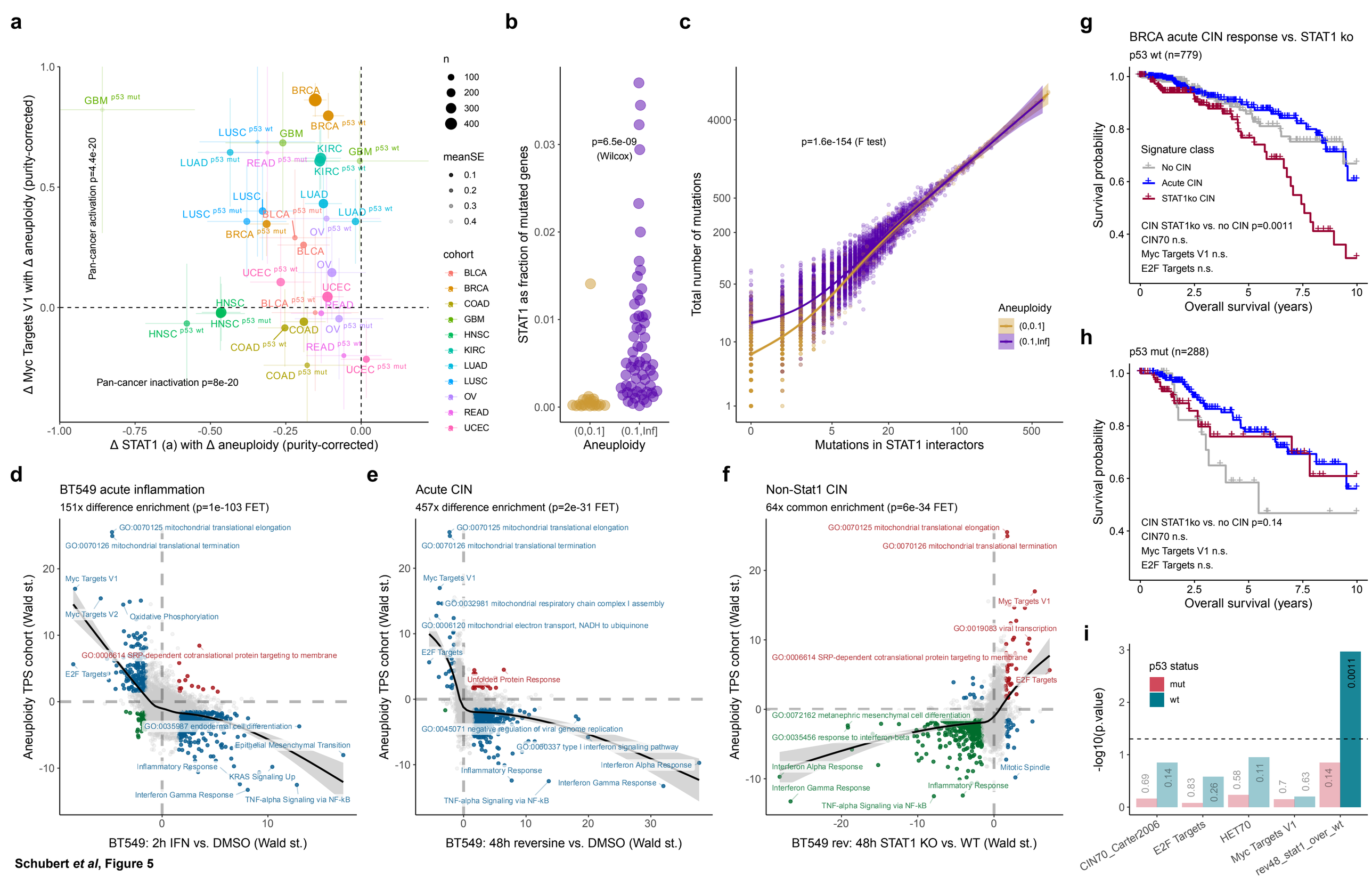

Schubert *et al*, Figure 5